Monthly Notices
of the
ROYAL ASTRONOMICAL SOCIETY

MNRAS **504,** 2877–2888 (2021)
Advance Access publication 2021 April 6

doi:10.1093/mnras/stab905

AB Aurigae: possible evidence of planet formation through the gravitational instability

James Cadman,[1,2]★ Ken Rice [1,2] and Cassandra Hall [3,4,5]

[1]*SUPA, Institute for Astronomy, University of Edinburgh, Blackford Hill, Edinburgh EH9 3HJ, UK*
[2]*Centre for Exoplanet Science, University of Edinburgh, Edinburgh EH9 3HJ, UK*
[3]*Department of Physics and Astronomy, The University of Georgia, Athens, GA 30602, USA*
[4]*Center for Simulational Physics, The University of Georgia, Athens, GA 30602, USA*
[5]*Department of Physics and Astronomy, University of Leicester, University Road, Leicester LE1 7RH, UK*

Accepted 2021 March 26. Received 2021 March 26; in original form 2021 February 12

ABSTRACT

Recent observations of the protoplanetary disc surrounding AB Aurigae have revealed the possible presence of two giant planets in the process of forming. The young measured age of 1–4 Myr for this system allows us to place strict time constraints on the formation histories of the observed planets. Hence, we may be able to make a crucial distinction between formation through core accretion (CA) or the gravitational instability (GI), as CA formation time-scales are typically Myr whilst formation through GI will occur within the first $\approx 10^4$–10^5 yr of disc evolution. We focus our analysis on the 4–13$M_{\rm Jup}$ planet observed at $R \approx 30$ AU. We find CA formation time-scales for such a massive planet typically exceed the system's age. The planet's high mass and wide orbit may instead be indicative of formation through GI. We use smoothed particle hydrodynamic simulations to determine the system's critical disc mass for fragmentation, finding $M_{\rm d,crit} = 0.3\,{\rm M}_\odot$. Viscous evolution models of the disc's mass history indicate that it was likely massive enough to exceed $M_{\rm d,crit}$ in the recent past; thus, it is possible that a young AB Aurigae disc may have fragmented to form multiple giant gaseous protoplanets. Calculations of the Jeans mass in an AB Aurigae-like disc find that fragments may initially form with masses 1.6–13.3$M_{\rm Jup}$, consistent with the planets that have been observed. We therefore propose that the inferred planets in the disc surrounding AB Aurigae may be evidence of planet formation through GI.

Key words: accretion, accretion discs – gravitation – instabilities – planets and satellites: formation – stars: formation.

1 INTRODUCTION

Most of the known exoplanets are believed to have formed in discs of gas and dust around young stars. Owing to recent advances in high-resolution infrared (IR) imaging we are now capable of observing the planet formation process taking place. Observations of these discs have revealed substructures indicative of the presence of planetary companions, such as rings (ALMA Partnership et al. 2015; Andrews et al. 2016; Avenhaus et al. 2018; Bertrang et al. 2018; Dipierro et al. 2018; Huang et al. 2018a), gaps (Andrews et al. 2011; Perez et al. 2015; Ginski et al. 2016; van Boekel et al. 2017), and spirals (Garufi et al. 2013; Grady et al. 2013; Benisty et al. 2015; Pérez et al. 2016; Tang et al. 2017; Dong et al. 2018; Huang et al. 2018b), and recently it has even become possible to directly image giant protoplanets forming (Keppler et al. 2018; Müller et al. 2018; Haffert et al. 2019; Boccaletti et al. 2020). Study of these systems may reveal crucial insights into the underlying physics governing the planet formation process.

AB Aurigae is a $2.4 \pm 0.2\,{\rm M}_\odot$, Herbig Ae/Be star (DeWarf et al. 2003), at a distance $d \approx 162.9 \pm 1.5$ pc (Gaia Collaboration et al. 2018). Various authors find an age for the star–disc system to be somewhere between 1 and 4 Myr (van den Ancker et al. 1997; DeWarf et al. 2003; Piétu, Guilloteau & Dutrey 2005). Measurements of the disc surrounding AB Aurigae find an extended, $R_{\rm out} = 400$–500 AU, low-mass disc, where $M_{\rm d} = 0.01\,{\rm M}_\odot$, with up to a factor of $\sim$10 uncertainty on the mass estimate (DeWarf et al. 2003; Andrews & Williams 2005; Corder, Eisner & Sargent 2005; Semenov et al. 2005). The stellar accretion rate of $\dot{M} = 1.3 \times 10^{-7}\,{\rm M}_\odot\,{\rm yr}^{-1}$ (Salyk et al. 2013) is unusually high for a 1–4 Myr old system, as the depleted disc mass at this late stage limits the available amount of accretable material.

The AB Aurigae disc has been studied extensively owing to its complex substructure, with authors reporting multiple rings (Piétu et al. 2005; Hashimoto et al. 2011; Tang et al. 2012, 2017), bright inner spirals (Piétu et al. 2005), extended CO spirals (Tang et al. 2012), and the possible presence of multiple, planetary-mass companions (Piétu et al. 2005; Tang et al. 2012, 2017). Recent high-resolution, scattered light observations of AB Aurigae performed by Boccaletti et al. (2020) using SPHERE provide some of the most spectacular images of a protoplanetary disc to date, revealing detailed spiral features, and placing new constraints on the properties of any potential companions. A kink in the inner spiral at $R \approx 30$ AU is found to be consistent with the presence of a protoplanet with mass of 4–13$M_{\rm Jup}$ (hereafter referred to as planet P1), which is also consistent with conclusions from previous authors (Piétu et al. 2005; Tang et al.

★ E-mail: cadman@roe.ac.uk

2012, 2017). The authors also report a point-source located at the outer edge of the inner disc, which is characterized by a gas and dust cavity at $R \approx 140$ AU, for which they tentatively derive a planetary mass of $3M_{\rm Jup}$ (hereafter referred to as planet P2). Throughout this paper, we aim to explore the likely formation history of planet P1.

In the core accretion (CA) model of giant planet formation (Mizuno 1980; Pollack et al. 1996), growth proceeds through the steady collisional accumulation of planetesimals on to a rocky core, which may eventually become massive enough for the onset of accretion of a gaseous envelope. Currently this model provides the most popular explanation for the formation of giant planets. However, it has been shown that formation time-scales, which may be anywhere up to 10 Myr, may exceed typical disc lifetimes (Haisch, Lada & Lada 2001), specifically in the case of giant planets on wide orbits where the planetesimal surface densities will be low. The discovery of systems such as HR 8799, where four ultra-wide-orbit ($15 < a < 70$ AU), super-Jupiter mass ($M_{\rm P} > 5M_{\rm Jup}$) planets have been directly imaged (Marois et al. 2008, 2010), is an example of a particularly challenging system to explain through *in situ* CA (Nero & Bjorkman 2009; Kratter, Murray-Clay & Youdin 2010).

CA also faces challenges when establishing how the first solids are able to grow up to and beyond metre sizes, as it is anticipated that grains will encounter growth barriers, such as the fragmentation (Birnstiel, Klahr & Ercolano 2012), bouncing (Zsom et al. 2010), and radial drift (Weidenschilling 1977) barriers. Mechanisms such as the streaming instability (Youdin & Goodman 2005; Youdin & Johansen 2007) may be capable of generating local regions of extremely high particle densities, which may then undergo gravitational collapse to form the first 100–1000 km planetesimals (Johansen et al. 2007). Dust trapping in the spiral regions of self-gravitating discs may also provide suitable conditions for accelerated growth (Rice et al. 2004), and possible fragmentation of the planetesimal disc (Rice et al. 2006). Multiwavelength IR observations of discs may allow us to probe their grain size distributions (Draine 2006; Williams & Cieza 2011; Dutrey et al. 2014; Testi et al. 2014; Ilee et al. 2020), place constraints on the rate of grain growth, and investigate whether significant growth may occur very early in the disc's evolution when it is massive enough to be self-gravitating (Dipierro et al. 2015; Cadman et al. 2020a).

In the gravitational instability (GI) model of planet formation (Boss 1997), unstable regions of the disc may directly collapse to rapidly form giant gaseous protoplanets and brown dwarfs. In a differentially rotating disc, susceptibility to GI can be determined by considering the Toomre Q parameter (Toomre 1964),

$$Q = \frac{c_{\rm s}\Omega}{\pi G \Sigma}, \tag{1}$$

where $c_{\rm s}$ is the local sound speed, Ω is the orbital frequency in a rotationally supported disc, G is the gravitational constant, and Σ is the local surface density. A disc may become susceptible to GI, the growth of spiral substructure, and potentially disc fragmentation, when $Q \lesssim 1.5$–1.7 (Durisen et al. 2007).

Fragmentation of the disc will occur if unstable regions are able to cool at a faster rate than the thermal energy is generated during collapse (i.e. if the cooling rate is greater than the heating rate). If the disc is able to cool rapidly, the instability will continue to grow until the inevitable outcome of fragmentation ensues. This requirement for rapid disc cooling, which can be characterized by a critical cooling rate (Gammie 2001; Rice, Lodato & Armitage 2005), demands that fragmentation will occur at large radii where the disc material is less optically thick, hence can cool more efficiently (Clarke 2009; Rice & Armitage 2009; Hall, Forgan & Rice 2017).

Calculation of the Jeans mass in a gravitationally unstable disc can be used to estimate the likely initial masses of fragments formed in this way. Using analytic approximations it has been shown that, with some dependence on the level of disc irradiation, fragmentation may initially form objects with masses between a few and a few tens of Jupiter masses (Forgan & Rice 2011, 2013a; Cadman et al. 2020b). Dynamical evolution, migration, tidal stripping, and growth will then follow, during which the fragment may contract to form a compact planetary/brown dwarf mass object, or be entirely torn apart and destroyed (Nayakshin 2010a,b, 2011; Forgan & Rice 2013b; Nayakshin & Fletcher 2015; Forgan et al. 2018; Humphries et al. 2019).

It has also been shown that discs around higher mass stars ($M_* \geq 2\,{\rm M}_\odot$) may be more susceptible to GI (Haworth et al. 2020; Cadman et al. 2020b), which is consistent with observations that show a higher occurrence rate of giant planets and brown dwarfs orbiting these systems (Johnson et al. 2007; Bowler et al. 2010; Nielsen et al. 2019). This suggested existence of two distinct populations of exoplanets is indicative of two modes of planet formation.

Although disc instability may not be a viable mechanism for directly forming many of the known exoplanets, it may play a role in the early growth of planet building material (Rice et al. 2004), as multifluid simulations of self-gravitating discs have shown significant enhancement of dust abundance present in spiral arms (Hall et al. 2020). It is possible, but still disputed, that it could also lead to the direct formation of the wide-orbit objects that are found via direct imaging (Vigan et al. 2017). We find ourselves in a unique position with AB Aurigae, as most of the exoplanets discovered to date have already undergone significant migration and dynamical evolution since their formation. The young age of AB Aurigae places strict time constraints on the possible formation histories of the observed planets; thus, it is an ideal site for testing theories of planet formation.

In this paper we focus on the formation history of planet P1 (CA versus GI), and whether it is possible that the AB Aurigae system could be evidence of planet formation through GI. This paper is organized as follows. In Section 2, we calculate the likely CA formation time-scale of planet P1, and in Section 3, we evaluate the possibility that the planet may have formed directly through GI during AB Aurigae's early evolution. We determine the critical disc-to-star mass ratio for fragmentation in Section 3.1, and use viscous evolution models in Section 3.2 to predict whether the disc may have ever been massive enough to fragment at some point in the recent past. We place new constraints on the current mass of the disc in Section 3.2.2, and in Section 3.3, we calculate the Jeans mass in a gravitationally unstable, AB Aurigae-like disc. We discuss our results and draw conclusions in Sections 4 and 5, respectively.

2 CORE ACCRETION

2.1 Core accretion time-scale

2.1.1 Methods

To model the formation time-scale of a gas giant planet through CA, we use a similar approach to that outlined in Ida & Lin (2004). We begin by assuming that either an $M_{\rm core,init} = 0.0$- or 0.1-$\rm M_\oplus$ core, with density $\rho_{\rm core} = 3.2\,{\rm g\,cm^{-2}}$, has formed at a semi-major axis, a, which we vary between 5 and 50 AU. For simplicity, we consider planet growth *in situ* and neglect any migration through the disc, the effect of which is discussed in Section 4.

Core growth proceeds at a rate (Safronov 1969),

$$\dot{M}_{\rm core} = \pi R_{\rm c}^2 \Sigma_{\rm p} \Omega f_{\rm g}, \tag{2}$$

where $R_{\rm c}$ is the radius of the core, $\Sigma_{\rm p}$ is the local planetesimal surface density, Ω is the angular frequency, and $f_{\rm g}$ is the gravitational enhancement factor, calculated using the equations from Greenzweig & Lissauer (1992). The local planetesimal surface density, $\Sigma_{\rm p}$, is defined as the surface density of dust within a radial annulus defined by the protoplanet's Hill radius, $R_{\rm H}$, where

$$R_{\rm H} = a \left(\frac{M_{\rm p}}{3 M_*} \right)^{1/3}, \tag{3}$$

where M_* is the mass of the host star and $M_{\rm p}$ is the total planet mass, equal to the sum of the core and envelope masses.

Whilst the core mass is still low, growth initially proceeds through planetesimal accretion, and we update $M_{\rm p}$ using equation (2) at each time-step. A planet may begin to retain a gaseous envelope if the core exceeds the critical mass for the onset of gas accretion, $M_{\rm crit}$, where (Ikoma, Nakazawa & Emori 2000)

$$M_{\rm crit} = 10 \left(\frac{\dot{M}_{\rm core}}{10^{-6}\,{\rm M}_\oplus\,{\rm yr}^{-1}} \right)^{0.25} \left(\frac{\kappa}{1\,{\rm g\,cm}^{-2}} \right)^{0.25} {\rm M}_\oplus, \tag{4}$$

where κ is the planetesimal opacity, for which we use $\kappa = 1\,{\rm g\,cm}^{-2}$.

We use a simple approach to calculate the accretion rate of a gaseous envelope on to the core, $\dot{M}_{\rm gas}$, based on the Kelvin–Helmholtz cooling time-scale, $\tau_{\rm KH}$, of the protoplanet, where

$$\tau_{\rm KH} = 10^9 (M_{\rm p}/{\rm M}_\oplus)^{-3} {\rm yr}, \tag{5}$$

and

$$\dot{M}_{\rm gas} = M_{\rm p}/\tau_{\rm KH}. \tag{6}$$

This approximation is only valid provided that there is sufficient disc gas present for the planet to accrete, and envelope accretion will cease if the planet is able to deplete all the gas available within its feeding zone. This can be defined in terms of an upper mass limit for *in situ* formation, known as the gas isolation mass, $M_{\rm g,iso}$, where

$$M_{\rm g,iso} = 50 \left(\frac{\Sigma_{\rm g}}{2400\,{\rm gcm}^{-2}} \right)^{1.5} \left(\frac{a}{1\,{\rm AU}} \right)^{3} \left(\frac{M_*}{{\rm M}_\odot} \right)^{-1/2} {\rm M}_\oplus, \tag{7}$$

where $\Sigma_{\rm g}$ is the local gas density. We prevent further growth once $M_{\rm p} \geq M_{\rm g,iso}$.

We set up the gas component of the disc with a total mass $M_{\rm gas} = 0.6\,{\rm M}_\odot$, hence a disc-to-star mass ratio, $q = 0.25$, and with $\Sigma_{\rm g} \propto R^{-1}$. The surface density profile of the gas disc is evolved using the one dimensional model outlined in Rice & Armitage (2009), where we assume a radially constant, fixed value for the Shakura–Sunyaev viscous-α of $\alpha = 10^{-3}$ (Shakura & Sunyaev 1973). The planetesimal component of the disc is set up as

$$\Sigma_{\rm p} = f_{\rm dust} \eta_{\rm ice} (R/R_0)^{-1}, \tag{8}$$

where $f_{\rm dust}$ is a scale factor such that we set $\Sigma_{\rm p}$ at 5 AU to be 2, 3, 5, and $10\,{\rm g\,cm}^{-2}$. $\eta_{\rm ice}$ is a constant where

$$\eta_{\rm ice} = \begin{cases} 4.2, & \text{if } a \geq a_{\rm ice} \\ 1, & \text{if } a < a_{\rm ice}, \end{cases} \tag{9}$$

and $a_{\rm ice}$ is the ice line located at

$$a_{\rm ice} = 2.7 (M_*/{\rm M}_\odot)^2 {\rm AU}. \tag{10}$$

In each case, we allow the planets to evolve in the disc for a maximum of 10 Myr.

2.1.2 Results

Fig. 1 illustrates the resultant planet growth tracks using this formalism, considering the setups with $M_{\rm core,init} = 0.01\,{\rm M}_\oplus$. Planet formation begins with a phase of core growth, which may either be slow or rapid depending on the local planetesimal surface density. This phase tends to plateau once the local planetesimal surface density is depleted, at which point the planet mass remains approximately constant. The critical core mass for the onset of gas accretion is proportional to the planetesimal accretion rate on to the core, and as the heating from accretion ceases the contraction of a gas envelope may ensue. Wide-orbit, giant planet formation is generally favoured near to, and just beyond the ice line due to the enhancement in the local planetesimal surface density. We calculate $a_{\rm ice} \approx 15.6$ AU for a star of mass $2.4\,{\rm M}_\odot$. If the local planetesimal surface density is particularly high, for example, near to the ice line in Fig. 1(c), the core mass may pass straight through the critical mass without plateauing. If the local planetesimal surface density is low, for example, at a large semi-major axis in Fig. 1(d), the core may never experience significant growth.

In Table 1, we show the results of 32 runs, where we measure the time for the core to have accreted a significant envelope, of mass equal to the core mass ($M_{\rm p} > 2M_{\rm core}$), and to reach a total planetary mass of $M_{\rm P1} = 4M_{\rm Jup}$, equal to the lower limit of the estimated mass for planet P1. We find it challenging to produce a planet of at least $4M_{\rm Jup}$ in an AB Aurigae-like disc in $\lesssim$ 1–4 Myr. In the majority of setups considered here, the planet will either reach its isolation mass before reaching the mass of planet P1, as seen in Fig. 1(a), or will not grow rapidly enough to reach $M_{\rm P1}$ within the duration modelled here. To rapidly form a planet this massive generally requires a significant core has initially formed, in a disc with an extremely high planetesimal surface density, with a planet on a shorter orbit than where planet P1 is currently located.

The planetesimal surface densities considered here, with $\Sigma_{\rm P,5\,AU} = 2$, 3, 5, and $10\,{\rm g\,cm}^{-2}$, correspond to total planetesimal masses across the disc of 0.012, 0.024, 0.048, and $0.072\,{\rm M}_\odot$, respectively. These are equivalent to initial dust-to-gas ratios of 0.01, 0.02, 0.04 and 0.06 if we assume that the dust and gas in the disc decoupled when the gas mass was $1.2\,{\rm M}_\odot$ (therefore when $q = 0.5$), and that all of this dust then went on to form planetesimals. However, if any of the dust was depleted by some other mechanism or did not go on to form planetesimals, which would likely be the case, then the planetesimal surface densities used here would demand much higher initial dust-to-gas ratio prior to decoupling. Therefore given the generously high planetesimal surface densities used here, we would consider these core accretion time-scales as optimistic lower limits to what we might expect in a realistic disc.

Mechanisms that may be capable of speeding up these core accretion time-scales and have not been included in the models here, such as pebble accretion, are discussed in Section 4.2.

3 THE GRAVITATIONAL INSTABILITY

Regions of a protoplanetary disc that become sufficiently gravitationally unstable may undergo a period of rapid collapse to directly form giant gaseous protoplanets and brown dwarfs. GI potentially offers an alternative formation mechanism for wide-orbit, giant planets whose formation time-scales are difficult to explain in the CA paradigm. Currently, it remains unclear whether GI may be a viable planet formation mechanism; it is uncertain whether discs may ever become sufficiently unstable to fragment, and if they are able to fragment

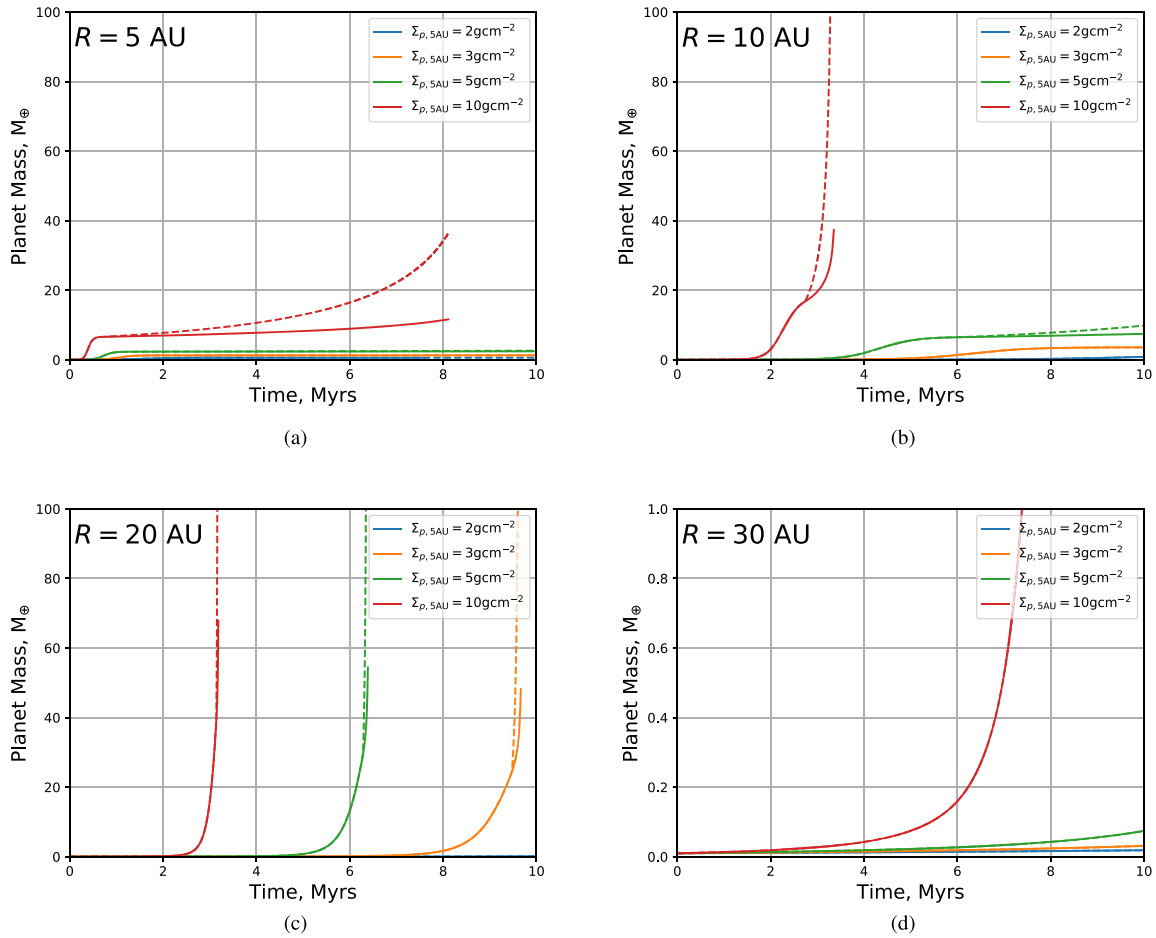

Figure 1. Evolution of planet core masses (solid line) and core + envelope masses (dashed lines) for *in situ* CA planet formation at radii $R = 5$ (1a), 10 (1b), 20 (1c), and 30 AU (1d) from the stellar host. In each case, the models begin with an initial core mass $M_{\rm core,init} = 0.01\,{\rm M}_\oplus$ at $t = 0$. We vary the planetesimal surface densities in the disc such that $\Sigma_{\rm P,5\,AU} = 2$, 3, 5, and 10 g cm^{-2}, which correspond to total planetesimal masses across the disc of 0.012, 0.024, 0.048, and 0.072 $\rm M_\odot$.

it may be that only stellar and brown dwarf-mass companions are capable of forming in this way.

3.1 Critical mass limit for fragmentation

3.1.1 Methods

We use the PHANTOM (Price et al. 2018) smoothed particle hydrodynamics (SPH) code to determine the critical mass limit for fragmentation in a disc around a 2.4-$\rm M_\odot$ star, analogous to AB Aurigae. SPH allows us to model the detailed hydrodynamics of a fluid, represented as N pseudo-particles, each with an assigned mass, position, velocity, and internal energy. A continuous fluid is approximated by calculating particle interactions through a Gaussian kernel function, with a characteristic smoothing length.

We represent the disc with $N = 1 \times 10^6$ SPH particles, distributed between $R_{\rm in} = 2.5$ and $R_{\rm out} = 400$ AU with a surface density profile $\Sigma \propto R^{-1}$ and sound speed profile $c_{\rm s} \propto R^{-0.25}$. We modify PHANTOM such that we model radiative cooling using the hybrid radiative transfer method outlined in Forgan et al. (2009), which combines the polytropic cooling formalism from Stamatellos et al. (2007) and the flux-limited diffusion method (Bodenheimer et al. 1990; Cleary & Monaghan 1999; Mayer et al. 2007). In using a combination of these two cooling methods, we model both the overall energy loss from the system and the detailed energy exchange between neighbouring particles at both high and low optical depths. We assume that disc irradiation leads to a constant background temperature, which we represent as, $T_{\rm irr} = 10$ K. Artificial disc viscosity is modelled using the standard $\alpha - \beta$ viscosity prescription, where we use $\alpha_{\rm SPH} = 0.1$ and $\beta_{\rm SPH} = 0.2$.

Each disc is allowed to evolve for a maximum of $t = 15,550$ yr, equal to three orbital periods at $R_{\rm out} = 400$ AU, or until fragments form and the computational time-step becomes prohibitively long for the simulations to continue. We calculate the thermalisation time-scale, $t_{\rm therm,i}$, from Forgan et al. (2009) for each of our disc final states, which represents the time for the disc material to reach thermal equilibrium. We find that in the discs that do not fragment within 15 550 yr, max $(t_{\rm ttherm,i}) \ll 1$ kyr. It is therefore reasonable to assume that if these discs have not fragmented after three orbital periods, they will not do so in future.

3.1.2 Results

Final states of these SPH simulations are shown in Fig. 2, where we vary the initial disc mass between 0.2 and 0.35 $\rm M_\odot$, which correspond to disc-to-star mass ratios $q = 0.08$–0.15.

Table 1. Results of the core accretion models.

$M_{\rm core,init}$ ($M_\oplus$) (1)	R (AU) (2)	$\Sigma_{\rm p,5\ AU}$ (g cm^{-2}) (3)	$t_{\rm env}$ (Myr) (4)	$t_{\rm P1}$ (Myr) (5)
0.01	5	2	–	–
0.01	5	3	–	–
0.01	5	5	–	–
0.01	5	10	6.43	–
0.01	10	2	–	–
0.01	10	3	–	–
0.01	10	5	–	–
0.01	10	10	3.14	–
0.01	20	2	–	–
0.01	20	3	9.56	–
0.01	20	5	6.33	–
0.01	20	10	3.16	3.18
0.01	30	2	–	–
0.01	30	3	–	–
0.01	30	5	–	–
0.01	30	10	8.77	8.82
0.1	10	2	–	–
0.1	10	3	–	–
0.1	10	5	–	–
0.1	10	10	1.88	–
0.1	20	2	6.81	–
0.1	20	3	3.95	4.05
0.1	20	5	2.60	2.66
0.1	20	10	1.30	1.32
0.1	30	2	–	–
0.1	30	3	9.92	–
0.1	30	5	6.61	6.72
0.1	30	10	3.33	3.38
0.1	50	2	–	–
0.1	50	3	–	–
0.1	50	5	–	–
0.1	50	10	–	–

Note. Columns are as follows: (1) initial core mass; (2) semi-major axis of core; (3) planetesimal surface density at 5 AU; (4) time before the planet reaches runaway growth, where the envelope mass exceeds the core mass; (5) time before the planet mass reaches $4M_{\rm Jup}$.

From the final states of these disc models, we expect a disc similar to AB Aurigae to fragment and form multiple clumps if $M_{\rm disc} \geq M_{\rm d,crit} = 0.3\,{\rm M}_\odot (q \geq 0.125)$, and to display non-axisymmetric substructure if $M_{\rm disc} \geq 0.25\,{\rm M}_\odot (q \geq 0.1)$. For $M_{\rm disc} \leq 0.2\,{\rm M}_\odot (q \leq 0.08)$, it is unlikely that the gravitational instability will lead to the growth of significant spirals and, in the absence of a perturber, it should be almost entirely axisymmetric. Therefore, given the current low-mass state of the AB Aurigae disc, we predict that it should be gravitationally stable, as expected.

When also considering a set of discs with outer radii $R_{\rm out} = 300$ and $R_{\rm out} = 500$ AU, we find that this critical disc-to-star mass ratio has some dependence on disc size, with more extended discs being more stable. When $R_{\rm out} = 500$ AU, we find the threshold for fragmentation at $M_{\rm d,crit} = 0.35\,{\rm M}_\odot (q_{\rm crit} = 0.15)$, and when $R_{\rm out} = 300$ AU, we find $M_{\rm d,crit} = 0.3\,{\rm M}_\odot (q_{\rm crit} = 0.125)$.

3.1.3 Subsequent migration of the clumps

Fragmentation will only occur if the disc is able to radiate energy away at a rate faster than the clump will collapse, hence primarily operates at large radii from the central star where the disc opacity is low thus it can cool efficiently. In the disc with $q = 0.125$, the fragment forms at $a \approx 200$ AU, much further out than the current semi-major axis of planet P1. 2D hydrodynamical simulations indicate that once fragments form in a gravitationally unstable disc, they will rapidly migrate to the inner regions within a few orbital periods (Baruteau, Meru & Paardekooper 2011). Computation times become prohibitively long for us to model the long-term migration of clumps in these simulations, as to resolve the high densities at the clump centres requires long integration times. Instead, typical migration of protoplanets can be approximated using the analytic calculations from Nayakshin (2010a). For type I migration, the time to move from radii $a_{\rm out}$ to $a_{\rm in}$ will be

$$\Delta t_{\rm mig,I} = \int_{a_{\rm out}}^{a_{\rm in}} \frac{t_{\rm mig,I(a)}}{a} {\rm d}a, \tag{11}$$

where

$$t_{\rm mig,I}(a) = \left(\frac{M_{\rm p}}{M_*}\Omega\right)^{-1} \frac{H}{a}, \tag{12}$$

and for type II migration,

$$\Delta t_{\rm mig,II} = \int_{a_{\rm out}}^{a_{\rm in}} \frac{t_{\rm mig,II(a)}}{a} {\rm d}a, \tag{13}$$

where

$$t_{\rm mig,II}(a) = \frac{1}{\alpha\Omega}\left(\frac{H}{a}\right)^{-2}, \tag{14}$$

where H is the disc scale height at $R = a$.

Whether a planet is in the type I or type II regime can be established in terms of a transition mass, $M_{\rm t}$, which roughly corresponds to the mass at which protoplanets become capable of gap-opening. For $M \leq M_{\rm t}$ (lower mass, faster migrating protoplanets), the planet will be in the type I regime, and for $M \geq M_{\rm t}$ (higher mass, slower migrating protoplanets), the planet will be in the type II regime, where

$$M_t = 2M_*\left(\frac{H}{R}\right)^3. \tag{15}$$

We can calculate the time for planet P1 to migrate from $a_{\rm out} = 200$ AU to $a_{\rm in} = 30$ AU, by substituting $M_* = 2.4\,{\rm M}_\odot$, $M_{\rm p} = 4M_{\rm Jup}$, $\alpha = 0.06$ for a saturated disc, and calculating the azimuthally averaged disc scale height, taken from the SPH disc where $M_{\rm disc} = 0.3\,{\rm M}_\odot$. Integrating equations (11) and (13), we calculate $\Delta t_{\rm mig,I} = 6.9$ kyr and $\Delta t_{\rm mig,II} = 1.0$ Myr. Note that the value of α used here should be considered an upper limit as α will decrease as the planet migrates. Thus, the calculated $t_{\rm mig,II}$ would be a lower limit.

From equation (15), we calculate the transition mass for gap opening to be $M_{\rm t} = 2.4M_{\rm Jup}$, which would place planet P1 comfortably in the type II regime. Baruteau et al. (2011), however, suggest that GI protoplanets will migrate inwards much faster than the gap opening time-scale, and that their migration may be better explained in the type I regime. $\Delta t_{\rm mig,I}$ and $\Delta t_{\rm mig,II}$ are likely more representative of lower and upper limits on the migration time-scale of planet P1, and the subsequent migration of a GI protoplanet will be best explained by a combination of both regimes. In either case, these simple calculations demonstrate that, to first approximation, it should be entirely possible for a fragment formed on a wide orbit to migrate inward to the current location of planet P1 within the lifetime of the AB Aurigae disc.

3.2 Viscous evolution models of AB Aurigae

Despite the system's disc mass being too low to be gravitationally unstable currently, it will likely have been much more massive in

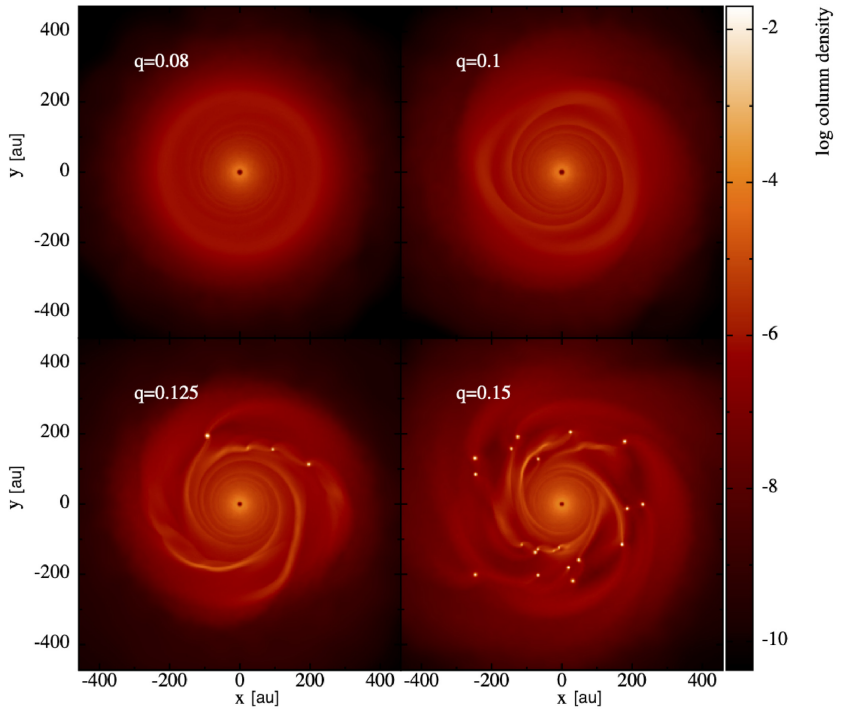

Figure 2. SPH models of an AB Aurigae-like disc. Each disc is set up with $M_* = 2.4\,\mathrm{M}_\odot$, $R_{\rm out} = 400$ AU, $N = 1 \times 10^6$ and $\Sigma \propto R^{-1}$, $c_{\rm s} \propto R^{-0.25}$. We vary the disc-to-star mass ratios within the range $q = 0.08$–0.15 ($M_{\rm d} = 0.2$–$0.35\,\mathrm{M}_\odot$). We find the critical disc-to-star mass ratio for fragmentation in an AB Aurigae-like disc to be $q_{\rm crit} = 0.125$ ($M_{\rm d,crit} = 0.3\,\mathrm{M}_\odot$).

the past prior to depletion by stellar accretion and photoevaporative winds, as massive discs will rapidly evolve away from an initially high-mass state (Hall et al. 2019). Viscous evolution models use analytic prescriptions to calculate the evolution history of a protoplanetary disc's surface density profile. Hence, we may use them to predict the mass evolution history of AB Aurigae.

3.2.1 Methods

Full details of the model used here to calculate the evolution of a disc whose primary source of viscosity is provided by self-gravity can be found in Rice & Armitage (2009). We also outline the basic equations here.

Viscous evolution of the surface density, $\Sigma(r, t)$, can be modelled using the one-dimensional prescription from Lynden-Bell & Pringle (1974) and Pringle (1981):

$$\frac{\partial \Sigma}{\partial t} = \frac{3}{r}\frac{\partial}{\partial r}\left[r^{1/2}\frac{\partial}{\partial r}(\nu \Sigma r^{1/2})\right] - \dot{\Sigma}_{\rm wind}, \tag{16}$$

where $\dot{\Sigma}_{\rm wind}$ represents the photoevaporative mass-loss due to radiation from the central star. Here we implement the X-ray photoionization model described in detail in Owen, Ercolano & Clarke (2011) and assume a moderate X-ray luminosity of $1 \times 10^{30}\,\mathrm{erg\,s^{-1}}$, noting that the rate of photoevaporative mass-loss scales linearly with X-ray luminosity. Disc viscosity, $\nu(r, t)$, is modelled using the Shakura–Sunyaev viscous-α prescription (Shakura & Sunyaev 1973),

$$\nu = \alpha c_{\rm s} H, \tag{17}$$

where the disc scale height, $H = c_{\rm s}/\Omega$, and $\Omega = \sqrt{GM_*/R^3}$ in a rotationally supported disc. The sound speed, $c_{\rm s}$, is calculated by solving equation (1), where we force the disc to be in a marginally unstable state with $Q = 1.5$.

The volume density can then be calculated as $\rho = \Sigma/2H$, and the temperature, T, optical depth, τ, and ratio of specific heats, γ, can be determined by interpolation of the equation of state table from Stamatellos et al. (2007) using the Rosseland mean opacities from Bell & Lin (1994).

To calculate the viscous-α term from equation (17), we must first determine the disc cooling time, which requires that we calculate the radiative cooling term (Hubeny 1990),

$$\Lambda = \frac{16\sigma}{3}\left(T^4 - T_{\rm irr}^4\right)\frac{\tau}{1+\tau^2}, \tag{18}$$

and determine the local cooling time as $t_{\rm cool} = U/\Lambda$, where the energy per unit surface area is

$$U = \frac{c_{\rm s}^2 \Sigma}{\gamma(\gamma - 1)}. \tag{19}$$

In a disc where the primary source of viscosity comes from self-gravity, the effective viscous-α term can be calculated as

$$\alpha = \frac{4}{9\gamma(\gamma-1)t_{\rm cool}\Omega}. \tag{20}$$

We set a lower limit, $\boldsymbol{\alpha_{\rm min}}$, below which we assume that GI is not the dominant source of viscosity but instead, in a sufficiently ionized disc, MRI may dominate, for example. If $\alpha < \alpha_{\rm min}$, we set $\alpha = \alpha_{\rm min}$ and recalculate the disc properties, now no longer requiring the disc to be gravitationally unstable with $Q = 1.5$.

Equations (1) and (20) can then be solved to calculate $c_{\rm s}$ and α for use in equation (17), and equation (16) can be integrated to determine the time evolution of the disc's surface density profile, hence its mass evolution.

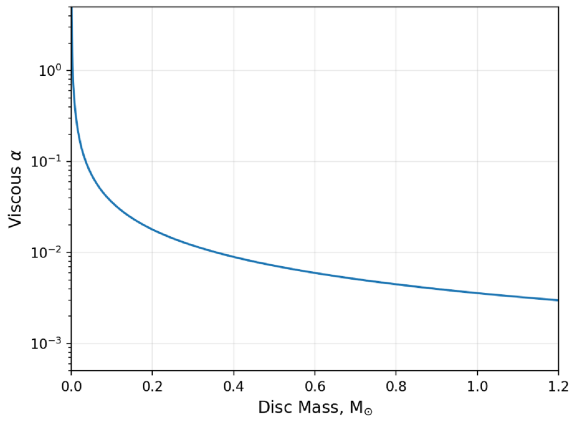

Figure 3. Viscous-α versus disc mass for a steady-state disc with $\dot{M} = 1.3 \times 10^{-7}\,\mathrm{M_\odot\,yr^{-1}}$, equal to the mass accretion rate measured in AB Aurigae. We calculate α as a function of disc mass using equation (23), which assumes that the disc has a radially constant viscous-α.

3.2.2 A note on the current mass of the AB Aurigae disc

Protoplanetary disc masses are notoriously challenging to measure. They often rely on empirical conversions between a disc's flux density and its mass, which requires uncertain assumptions about the disc optical depth, metallicity, dust-to-gas ratio, and grain size distribution. Combined with uncertainties in the flux measurement and distance toward the system, mass estimates may be uncertain by up to an order of magnitude, and are usually considered to represent lower bounds. Estimates of the disc mass surrounding AB Aurigae find a low-mass disc, with $M_\mathrm{d} = 0.01\,\mathrm{M_\odot}$ and uncertainty up to a factor of ≈10 (Andrews & Williams 2005; Corder et al. 2005; Piétu et al. 2005; Semenov et al. 2005).

The accretion rate on to the star may also provide us a with rough estimate of the disc mass, as it is indicative of the mass reservoir available to the star from the disc. A protoplanetary disc is expected to settle into a steady state with a constant mass accretion rate (Pringle 1981),

$$\dot{M} = \frac{3\pi\alpha c_\mathrm{s}^2 \Sigma}{\Omega} = \text{constant}. \tag{21}$$

In a disc with sound speed profile, $c_\mathrm{s} = c_{\mathrm{s},0} R^{-0.25}$, and surface density profile, $\Sigma = \Sigma_0 R^{-1}$, the disc may have a radially constant viscous-α given by

$$\alpha = \frac{1}{3\pi} \frac{\dot{M}\sqrt{GM_*}}{c_{\mathrm{s},0}^2 \Sigma_0}. \tag{22}$$

We can substitute in for $c_{\mathrm{s},0}$ by assuming a flattened disc with $H/R = 0.1$ at $R = 100\,\mathrm{AU}$, and substituting $H = c_\mathrm{s}/\Omega$, where H is the local disc scale height. Similarly, we can substitute Σ_0 for the disc outer radius, $R_\mathrm{out} = 400\,\mathrm{AU}$, and disc mass to obtain an equation in terms of α and M_d:

$$\alpha = \frac{200}{3} \frac{\dot{M} R_\mathrm{out}}{\sqrt{GM_*}} \frac{\sqrt{100\,\mathrm{AU}}}{M_\mathrm{d}}. \tag{23}$$

We plot this equation in Fig. 3 for a star of mass $2.4\,\mathrm{M_\odot}$ and mass accretion rate $\dot{M} = 1.3 \times 10^{-7}\,\mathrm{M_\odot\,yr^{-1}}$ (Salyk et al. 2013). In Table 2 we show calculated disc masses corresponding to α values 0.1, 0.01 and 0.001.

From Fig. 3, we see that for a very-low mass disc ($M_\mathrm{d} \leq 0.1\,\mathrm{M_\odot}$) to have an accretion rate $\dot{M} = 1.3 \times 10^{-7}\,\mathrm{M_\odot\,yr^{-1}}$ would require a disc viscosity much higher than we would usually expect from a quasi-stable disc, with $\alpha \geq 0.1$. If instead the disc is still massive, with $M_\mathrm{d} \geq 0.1\,\mathrm{M_\odot}$, the viscous-$\alpha$ required to explain the high accretion rate drops significantly. In a quasi-stable disc, we might typically expect $\alpha \approx 10^{-2}$–10^{-4} (Hartmann et al. 1998; Rafikov 2017).

We do not attempt to propose an exact disc mass for AB Aurigae here, but instead wish to highlight that in order to explain the system's high accretion rate may require that the disc is more massive than has previously been suggested, and that it is likely at least as massive as the upper bound of the current disc mass estimates.

Table 2. Disc masses corresponding to $\alpha = 0.1$, 0.01, and 0.001 in Fig. 3.

α	M_disc ($\mathrm{M_\odot}$)
0.1	0.04
0.01	0.36
0.001	>1.2

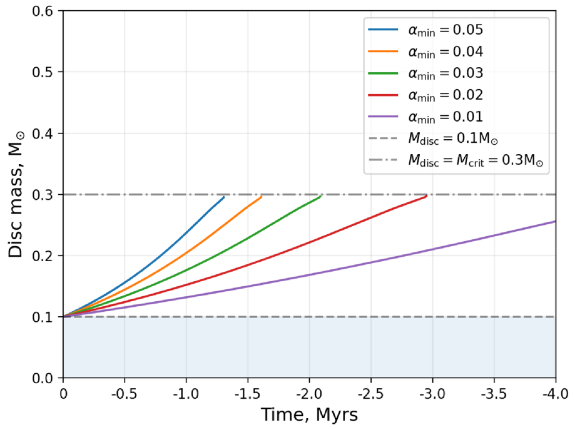

Figure 4. The mass evolution of a disc similar to AB Aurigae, calculated using the viscous evolution models outlined in Section 3.2.1. The plot begins with a disc mass equal to the current mass of AB Aurigae, with $M_\mathrm{d} = 0.1\,\mathrm{M_\odot}$ at $t = 0$, and illustrates how long in the recent past the disc mass may have exceeded the critical mass limit for fragmentation, $M_\mathrm{d,crit} = 0.3\,\mathrm{M_\odot}$. Hence, the x-axis measures Myr in the past. We vary the value of α_min, which represents a background viscous-α value generated by some process other than disc self-gravity.

3.2.3 Results

With this in mind we use these viscous evolution models to predict how long ago the AB Aurigae disc may have been massive enough to exceed the critical mass limit for fragmentation, where $M_\mathrm{d} = M_\mathrm{crit} = 0.3\,\mathrm{M_\odot}$, assuming the system to have a current disc mass approximately equal to the upper bound on the mass estimate, $M_\mathrm{d} = 0.1\,\mathrm{M_\odot}$.

In order to do this, we set up discs with initial masses $M_\mathrm{d} = M_\mathrm{crit} = 0.3\,\mathrm{M_\odot}$ and evolve them forward in time until their mass has been depleted to $M_\mathrm{d} = 0.1\,\mathrm{M_\odot}$, assuming α_min values in the range 0.01–0.05. Discs are set up with initial parameters similar to what we might expect in a young AB Aurigae disc, with $M_* = 2.4\,\mathrm{M_\odot}$, $R_\mathrm{out,init} = 400\,\mathrm{AU}$, surface density profile $\Sigma \propto R^{-1}$, and temperature profile $T \propto R^{-0.75}$. We assume again that irradiation leads to a constant background temperature $T_\mathrm{irr} = 10\,\mathrm{K}$.

The results of these models are shown in Fig. 4. To illustrate how long in the recent past the AB Aurigae disc may have been massive

enough to exceed the fragmentation threshold, we have plotted the disc mass evolution in reverse order. Hence, $t = 0$ represents the disc in its current state, with $M_{\rm d} = 0.1\,{\rm M}_{\odot}$, and the x-axis measures Myr in the past. For example, in the case of the $\alpha_{\rm min} = 0.05$ model, we predict that the AB Aurigae disc may have been more massive than $M_{\rm d,crit} = 0.3\,{\rm M}_{\odot}$, approximately 1.3 Myr ago. This approach is equivalent to if we had run the models in Section 3.2.1 backwards, beginning at $M_{\rm d} = 0.1\,{\rm M}_{\odot}$.

Discs with higher viscous−α values will evolve at a faster rate, hence the time between the disc mass being in its current state, with $M_{\rm d} = 0.1\,{\rm M}_{\odot}$, and exceeding the critical mass limit, $M_{\rm d,crit} = 0.3\,{\rm M}_{\odot}$, will be shorter.

These models again reiterate how it is challenging to reconcile the current low estimated disc mass with the high measured accretion rate, leading us to conclude that AB Aurigae is either currently more massive than observations suggest, or was almost certainly so in its recent past. In the highest accreting case, with $\alpha_{\rm min} = 0.05$, we find the accretion rate when $M_{\rm d} = 0.1\,{\rm M}_{\odot}$ to be $\dot{M} = 4.80 \times 10^{-8}\,{\rm M}_{\odot}\,{\rm yr}^{-1}$, and in the lowest accreting case with $\alpha_{\rm min} = 0.01$, we find $\dot{M} = 9.0 \times 10^{-8}\,{\rm M}_{\odot}\,{\rm yr}^{-1}$, both of which are significantly lower than the currently measured value of $\dot{M} = 1.3 \times 10^{-7}\,{\rm M}_{\odot}\,{\rm yr}^{-1}$ (Salyk et al. 2013).

Crucially though, the plots in Fig. 4 demonstrate how we can trace the AB Aurigae disc back to a previously higher mass state, and how the disc mass may have exceeded the fragmentation threshold in the recent past. When assuming a moderate background $\alpha_{\rm min}$, we find that the disc mass may have exceeded $M_{\rm d,crit}$ within the past ≈1.25–4 Myr. Thus, it is plausible that a young AB Aurigae disc may have fragmented to form one or multiple giant gaseous protoplanets during its early evolution.

3.3 Jeans mass in an AB Aurigae-like disc

The local Jeans mass in a self-gravitating disc can be used, in the case where a region of the disc fragments, to estimate the masses of the bound clumps that will form. Cadman et al. (2020b) derived a revised equation for the Jeans mass in an irradiated self-gravitating disc (presented in its original form in Forgan & Rice 2013a) given by

$$M_{\rm J} = \frac{\sqrt{3}}{32G}\frac{\pi^3 Q^{1/2} c_{\rm s}^2 H}{(1 + 4.47\sqrt{\alpha})^{1/2}}. \quad (24)$$

We can use the same approach as in Section 3.2.1 to calculate how the Jeans mass varies as a function of $\dot{M}$ and $R_{\rm out}$. We assume the disc to be marginally unstable, with $Q = 1.5$, and use equation (1) to obtain $c_{\rm s}$, and solve equation (20) to obtain α for use in equation (21), allowing us to calculate the Jeans mass for a range of disc outer radii and accretion rates.

In Fig. 5, we plot equation (24), for a disc around a 2.4-${\rm M}_{\odot}$ star, with $\dot{M}$ between 1×10^{-9} and $1 \times 10^{-4}\,{\rm M}_{\odot}\,{\rm yr}^{-1}$, and $R_{\rm out}$ between 50 and 500 AU. We assume that disc irradiation leads to a constant background temperature, and consider two cases where $T_{\rm irr} = 10$ and 50 K. Higher disc temperatures reduce the effective viscous-α from equation (20) for discs of the same mass, whilst also providing greater pressure support against direct collapse, thus stabilizing the system against GI. Hence, for a given $\dot{M}$ and $R_{\rm out}$ the Jeans mass increases as a function of irradiation.

A gravitationally unstable disc may fragment if a collapsing clump is able to cool and radiate energy away at a rate faster than the local dynamical time. This condition can be expressed in terms of a critical value of the dimensionless cooling parameter, $\beta_{\rm c} = t_{\rm cool}\Omega$, which, in turn, can be expressed in terms of a critical viscous-α (see equation 20). We typically expect this value to be somewhere between $\alpha_{\rm crit} \approx 0.06$ and 0.1 (Gammie 2001; Rice et al. 2005; Baehr, Klahr & Kratter 2017); thus, we include contours of $\alpha = 0.01$ and 0.1 in Fig. 5 to indicate regions of the parameter space that may fragment.

These plots reiterate that at an earlier stage of AB Aurigae's evolution, when the mass accretion rate was likely higher than it currently is, it is entirely plausible that the disc may have been gravitationally unstable and may have fragmented, as these higher accretion rate states lie in an unstable region of parameter space.

For a given disc radius, the minimum Jeans mass doesn't vary much whether we assume fragmentation can only occur for $\alpha \geq 0.01$ or $\alpha \geq 0.1$. Assuming that $\alpha_{\rm crit} = 0.1$, we find the minimum Jeans masses at $R = 200$, 300, and 400 AU to be 1.6, 2.5, and $3.4 M_{\rm Jup}$, respectively, when $T_{\rm irr} = 10$ K, and to be 10.3, 12.4, and $13.3 M_{\rm Jup}$, respectively, when $T_{\rm irr} = 50$ K, roughly coinciding with what we observe from the mass of planet P1.

4 DISCUSSION

4.1 Implications for formation through CA

Significant fine tuning of the model parameters is required in Section 2 to form planet P1 through CA within the strict time constraint of the system's measured age. To form a planet of $4 M_{\rm Jup}$ within 1–4 Myr generally requires a planetesimal surface density much higher than would usually be expected, with a total planetesimal mass across the disc $\geq 0.072\,{\rm M}_{\odot}$ when $M_{\rm core,init} = 0.01\,{\rm M}_{\odot}$, and $\geq 0.024\,{\rm M}_{\odot}$ when $M_{\rm core,init} = 0.1\,{\rm M}_{\odot}$. When $\Sigma_{\rm p,5\,AU} = 2\,{\rm g\,cm}^{-2}$, hence with a total planetesimal mass across the disc of $0.012\,{\rm M}_{\odot}$, we generally see very slow planet growth.

It is important to note however that we have only considered a simple formalism for our modelling of CA here, and that processes not included in our models, such as planet migration, pebble accretion, and disc instabilities, may be capable of accelerating initial growth. We discuss the effect of these next.

4.2 Limitations of the CA models

Migration allows the planet to sample a wider region of the disc, therefore preventing the local planetesimal surface density becoming depleted as rapidly as when it grows *in situ*. When we include core migration in Section 2, the planets generally grow at a faster rate. However, we chose to only consider *in situ* formation here, as including migration causes all the cores to migrate to the inner disc ($a \lesssim 3$ AU) away from the location where we currently find planet P1, and toward the regions of higher planetesimal surface density where they accrete at a faster rate. Some other mechanism, such as planet–planet scattering, would then be required to explain planet P1's subsequent migration out to $a \approx 30$ AU. When modelling *in situ* formation at the current semi-major axis of planet P1, we see only slow growth when $M_{\rm core,init} = 0.1\,{\rm M}_{\oplus}$, and almost no growth when $M_{\rm core,init} = 0.01\,{\rm M}_{\oplus}$.

Instabilities in discs may be capable of generating large over-densities of solids, hence they have been suggested as possible mechanisms for accelerated planetesimal growth and, in extreme cases, fragmentation of the disc solids under their self-gravity. The spiral arms of young, GI discs have been shown to cause strong dust-trapping (Rice et al. 2004), whilst the gravitational collapse of filaments generated in the streaming instability (Youdin & Goodman 2005; Youdin & Johansen 2007) may form planetesimals of radii 100–1000 km (Johansen et al. 2007; Johansen, Klahr & Henning

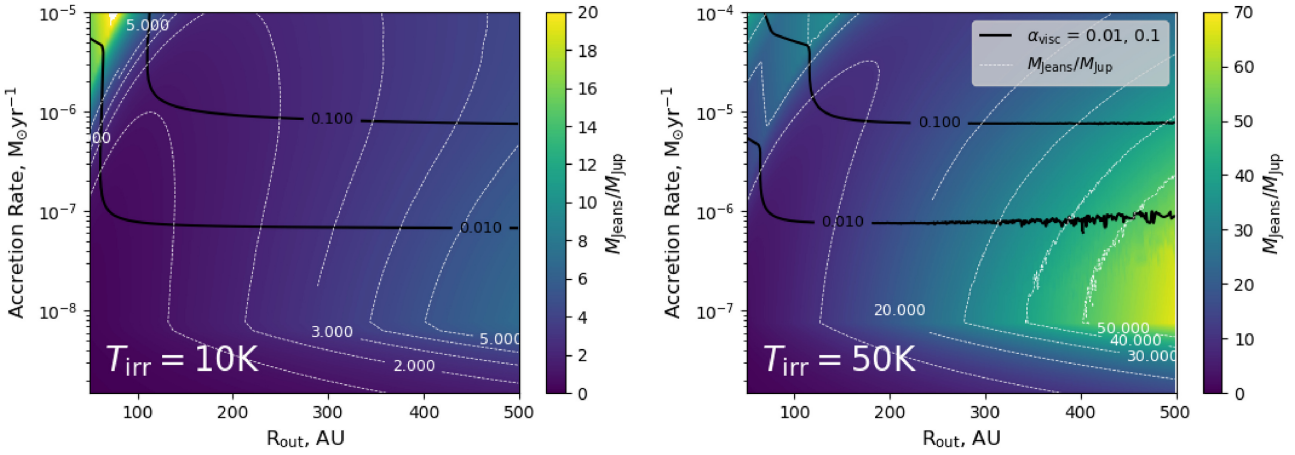

Figure 5. The Jeans mass in a self-gravitating disc surrounding a 2.4-$M_\odot$ star. We consider two cases of disc irradiation, one where it leads to constant background temperature of $T_{irr} = 10$ K (left-hand panel) and one where it leads to constant background temperature of $T_{irr} = 50$ K (right-hand panel). We expect a disc to be unstable against fragmentation for $\alpha_{crit} \approx 0.06$–$0.1$; thus, we plot contours of $\alpha = 0.01$ and 0.1 to indicate regions of parameter space that would likely be unstable against fragmentation. Higher temperatures act to stabilize the disc against the gravitational instability by reducing the effective-α. Hence, for a given $\dot{M}$ and R_{out}, the Jeans masses will be higher when $T_{irr} = 50$ K compared to when $T_{irr} = 10$ K.

2011; Johansen, Youdin & Lithwick 2012), thus providing a possible mechanism for the initial formation of rocky cores. Whilst refraining from modelling the detailed physics of dust trapping through disc instabilities, we can crudely represent local grain enhancements by simply increasing the total dust-to-gas ratio in the disc, which by default will increase the planetesimal surface density local to the accreting core. We account this by increasing the total planetesimal surface density by up to a factor of 6 in Section 2.

Mechanisms for accelerated growth and rapid core formation become necessary as CA faces challenges when establishing how the first planetesimals are able to grow beyond metre sizes. The initial stages of growth are believed to be slow, as dust grains may encounter growth barriers beyond metre sizes (Brauer, Dullemond & Henning 2008; Mordasini et al. 2010). It has been shown, as a consequence of intrinsic gas-dust drag in the disc, that grains of a critical size will radially migrate and be accreted on to the star within a fraction of the disc lifetime (the radial drift barrier, Weidenschilling 1977). Further, solids of millimetre to centimetre sizes, with Stokes number close to 1, are expected to have high relative azimuthal velocities; hence, grain–grain collisions may become destructive, resulting in shattering (the fragmentation barrier (Birnstiel et al. 2012), or neutral and result in recoiling (the bouncing barrier; Zsom et al. 2010), both of which prevent a positive outcome of coagulation. In our model we assume that a core of mass 0.01 or 0.1 $M_\oplus$, with $R_{core,init} = 1.6 \times 10^3$ and 3.5×10^3 km, respectively, has already formed at $t = 0$, therefore avoiding the detailed physics of this initial phase of core growth. Note that these initial core sizes are consistent with, but slightly larger than, the planetesimals expected to form through direct collapse of the dust disc during the streaming instability (Johansen et al. 2007, 2011, 2012).

Possibly most importantly, we note that we do not include a prescription for pebble accretion in our model (for a review see Johansen & Lambrechts 2017). Accretion of millimetre to centimetre sized pebbles on to planetesimal cores may have the potential to generate significantly faster growth rates than the planetesimal-planetesimal accretion we consider here. Pebbles may be abundant in protoplanetary discs, since it is a natural outcome from the fragmentation and bouncing barriers. Pebbles of millimetre-centimetre sizes are coupled to the gas in the disc. The gas component orbits at sub-Keplerian velocities due to the outward gas pressure. The solids, which are orbiting at Keplerian velocities, will experience a drag force that, in a smooth, laminar disc, will cause them to radially drift inward. This migration of pebbles can lead to them being transported to within the path of the growing planetesimal core, constantly replenishing the pebbles within the planetesimal's feeding zone and preventing it from reaching its isolation mass as quickly as they do in Section 2. If the planetesimal is gravitationally massive and capable of perturbing the velocities of nearby solids, the pebbles may enter into complex trajectories, orbiting and eventually settling down into its gravitational potential well. If the planetesimal's gravitational cross-section exceeds its geometric cross-section, pebble accretion may become the dominant growth mechanism. In their review paper Johansen & Lambrechts (2017) show that pebble accretion may be capable of resolving many of the time-scale problems associated with CA, whilst being able to explain the formation of all planet types.

4.3 Implications for formation through GI

In Section 3.1, we used SPH simulations to determine the critical mass limit for fragmentation in a disc surrounding a 2.4-$M_\odot$ star, finding that for an $R_{out} = 400$ AU disc, $M_{d,crit} = 0.3\,M_\odot$ ($q_{crit} = 0.125$). Whilst we have mostly focused our discussion on the case of single fragment formation from our SPH simulations, it is also likely that multiple clumps may form in a disc with a mass slightly higher than $M_{d,crit}$ (see Fig. 2). The initial formation of multiple protoplanets may then also provide an explanation for the wider-orbit planet P2 that has also been inferred, located at a distance $a \approx 140$ AU from the parent star (Boccaletti et al. 2020). We have refrained from analysing the formation history of planet P2, due to its slightly more tentative detection, choosing instead to focus on planet P1. However, it would seem that the formation of a 3-M_{Jup} planet at $a \approx 140$ AU may be even more challenging to explain in the CA paradigm than is the case for planet P1, as the gas and dust surface densities in the disc will drop off as $\Sigma \propto R^{-1}$, hence will be exceedingly low at such a large radius. As we see only minimal core growth at $R = 30$ AU in Fig. 1(d), it is

likely that growth at $R = 140$ AU would be near-negligible. It may then be the case that in fact planets P1 and P2 represent two survivors from several fragments that could have initially formed.

Despite the AB Aurigae disc being far too low mass to be gravitationally unstable currently, models of the system's viscous evolution in Section 3.2 suggest that it may have been much more massive when it was younger, potentially exceeding the critical mass limit for fragmentation. It seems reasonable to expect that the disc might have previously fragmented in an extended system such as AB Aurigae, as previous studies suggest that fragmentation is inevitable in GI discs at radii, $R \gtrsim 50$–100 AU (Rafikov 2005; Whitworth & Stamatellos 2006; Clarke 2009; Forgan & Rice 2011). Further, Cadman et al. (2020b) and Haworth et al. (2020) used hydrodynamic simulations to demonstrate that, whilst lower mass stars may support gravitationally stable massive discs, susceptibility to fragmentation increases as a function of stellar mass, and that discs around higher mass stars ($M_* \geq 2\,\mathrm{M}_\odot$) may fragment for relatively low disc-to-star mass ratios. AB Aurigae being an extended disc around a higher mass star therefore seems to be an ideal candidate system to search for surviving products of GI.

If the disc had been able to fragment whilst it was young, it is not necessarily true that the clumps will have survived the 1–4 Myr lifetime of the AB Aurigae system. We find that fragments may initially form on wide orbits with $R \gtrsim 200$ AU, and use analytic calculations to predict initial clump masses 1.6–$13.3 M_{\mathrm{Jup}}$. However, subsequent evolution is inevitable, and the fragments will rapidly migrate through the disc (Baruteau et al. 2011).

In the tidal downsizing hypothesis of planet formation (Nayakshin 2010a,b, 2011), GI embryos will cool and contract as they migrate. Dust sedimentation may lead to the formation of a solid core, potentially of mass comparable to that of a terrestrial planet (Boss 1998). If the embryo's outer layers contract slowly whilst migration occurs rapidly then tidal stripping from the parent star may occur once the embryo reaches the inner disc, as its physical radius may exceed its Hill sphere (Nayakshin 2010a). It is possible that many of the initially formed fragments may be entirely destroyed during this tidal downsizing process (Nayakshin & Fletcher 2015; Humphries et al. 2019). Population synthesis calculations find this may be the true of ≈ 50 per cent of GI protoplanets, with the remaining objects eventually residing at $a \gtrsim 20$ AU (Forgan & Rice 2013b), although when including fragment-fragment scattering this survival fraction may be significantly less (Forgan et al. 2018). The initial formation of multiple clumps would then be necessary if any are to survive beyond this early phase of evolution. Accretion of material on to the protoplanets will also occur as they migrate through the disc. Kratter et al. (2010) showed that most GI fragments will grow well beyond the mass limit for Deuterium burning, and that any GI-born planets likely represent the low mass tail of the eventual GI fragment mass distribution. The Jeans mass estimates that we present in Section 3.3 therefore represent those shortly after collapse only, as dynamical evolution will significantly influence the embryo's eventual mass.

We also tentatively suggest that the previous disc mass estimates ($M_{\mathrm{d}} \approx 0.01\,\mathrm{M}_\odot$; DeWarf et al. 2003; Andrews & Williams 2005; Corder et al. 2005; Semenov et al. 2005) appear too low to be consistent with the high stellar accretion rate (Salyk et al. 2013), which is indicative of the presence of a large mass reservoir. Assuming the disc to be in a quasi-steady state with a radially constant viscous–α suggests a lower limit for the current disc mass as $M_{\mathrm{d}} \gtrsim 0.1\,\mathrm{M}_\odot$ (see Fig. 3). This rough lower limit is in fact consistent with the upper bound of the uncertainty on the current disc mass estimates. However even when assuming this slightly higher disc mass, we still find the calculated accretion rates from our viscous evolution models in Section 3.2.3 to be significantly lower than the accretion rate measured from the system. On the unusually high stellar accretion rate, Tang et al. (2012) suggest a possible explanation is the presence of an inner disc, characterized by a gas/dust cavity observed at $R \approx 100$ AU, which is being replenished through accretion from the remnant envelope above and below the disc mid-plane. This would suggest that the measured accretion rate does not represent that of a settled, $R_{\mathrm{out}} = 400$ AU disc as we have assumed here, and would allow for the existence of a low-mass disc whilst being consistent with a high accretion rate. We only attempt to further highlight this discrepancy between the measured disc mass and accretion rate, and note that the current mass of the disc does not significantly affect the overall conclusions from this paper in regards to the formation history of planet P1.

5 CONCLUSIONS

In this paper, we have analysed the possible formation history of the 4–$13 M_{\mathrm{Jup}}$ planet observed at $a \approx 30$ AU within the protoplanetary disc surrounding AB Aurigae (Piétu et al. 2005; Tang et al. 2012, 2017; Boccaletti et al. 2020). The young age of the star–disc system places strict constraints on the CA formation time-scale, which we find challenging to explain within 1–4 Myr. The planet's high mass and wide orbit are indicative of a planet that may have instead formed through disc instability in the natal AB Aurigae disc.

The key results are as follows:

(i) Typical *in situ* CA formation time-scales for planet P1 exceed the system's measured age. Fine tuning of the model parameters is required in order to form a planet of $4 M_{\mathrm{Jup}}$ within 1–4 Myr, including significant enhancement of the planetesimal surface density in the disc, and, in most cases, that a large planetesimal core with $M_{\mathrm{core,init}} = 0.1\,\mathrm{M}_\oplus$ has already formed near to the snow line at $t = 0$. At the current semi-major axis of planet P1 ($a = 30$ AU), we find extremely slow *in situ* growth due to the low disc surface densities at wide orbits. We do not include a prescription for pebble accretion in our models here, but note that it may be capable of speeding up planet growth.

(ii) A disc surrounding a 2.4-$\mathrm{M}_\odot$ star, analogous to young AB Aurigae, would have fragmented if its initial mass exceeded $M_{\mathrm{d,crit}} = 0.3\,\mathrm{M}_\odot$ ($q_{\mathrm{crit}} = 0.125$). If the disc mass is slightly higher than $M_{\mathrm{d,crit}}$, several fragments may form. Formation of multiple fragments would allow margin for some fragment destruction, which is likely inevitable during their subsequent dynamical evolution of GI protoplanets.

(iii) Viscous evolution models of the AB Aurigae disc suggest that it may have been massive enough to exceed $M_{\mathrm{d,crit}}$ during its early evolution whilst the disc was still young and massive. We find that a 0.1-$\mathrm{M}_\odot$ disc may have exceeded $M_{\mathrm{d,crit}} = 0.3\,\mathrm{M}_\odot$ within the past $\approx$1.25–4 Myr when considering moderate background viscosity.

(iv) Fragments will initially form on wide orbits, where the disc material is cool, and then rapidly migrate inwards. Typical migration time-scales of a GI protoplanet that formed at $R \approx 200$ AU within a young AB Aurigae disc are found to be shorter than the current age of the system. We use analytic calculations to determine type I and type II migration time-scales, finding that for migration from $R_{\mathrm{out}} = 200$ AU to $R_{\mathrm{in}} = 30$ AU, $\Delta t_{\mathrm{mig,I}} = 6.9$ kyr, and $\Delta t_{\mathrm{mig,II}} = 1.0$ Myr when considering disc conditions taken from our hydrodynamic simulations.

(v) Calculations of the Jeans mass in a moderately irradiated proto-AB Aurigae disc represent what the initial fragment masses might

have been immediately after formation. We find that $M_J = 1.6$–$13.3 M_{Jup}$, which is consistent with the masses of the planets P1 and P2 in the AB Aurigae disc.

(vi) Although we focus our discussion on the formation history of planet P1, we highlight that planet P2 found at $a \approx 140$ AU with an estimated mass $M_{P2} = 3 M_{Jup}$ may be even more challenging to reconcile with formation through CA.

We therefore propose that planets P1 and P2 that have been inferred through scattered light observations of the AB Aurigae disc (Boccaletti et al. 2020) may stand as evidence of planet formation through GI.

ACKNOWLEDGEMENTS

JC would like to acknowledge funding from a Higgs scholarship provided by the Scottish Funding Council. CH is a former Winton Fellow and part of this work was supported by Winton Philanthropies/The David and Claudia Harding Foundation.

DATA AVAILABILITY

The model data generated in this study will be shared on request to the corresponding author.

REFERENCES

ALMA Partnership et al., 2015, ApJ, 808, L3
Andrews S. M. et al., 2016, ApJ, 820, L40
Andrews S. M., Williams J. P., 2005, ApJ, 631, 1134
Andrews S. M., Rosenfeld K. A., Wilner D. J., Bremer M., 2011, ApJ, 742, L5
Avenhaus H. et al., 2018, ApJ, 863, 44
Baehr H., Klahr H., Kratter K. M., 2017, ApJ, 848, 40
Baruteau C., Meru F., Paardekooper S.-J., 2011, MNRAS, 416, 1971
Bell K. R., Lin D. N. C., 1994, ApJ, 427, 987
Benisty M. et al., 2015, A&A, 578, L6
Bertrang G. H. M., Avenhaus H., Casassus S., Montesinos M., Kirchschlager F., Perez S., Cieza L., Wolf S., 2018, MNRAS, 474, 5105
Birnstiel T., Klahr H., Ercolano B., 2012, A&A, 539, A148
Boccaletti A. et al., 2020, A&A, 637, L5
Bodenheimer P., Yorke H. W., Rozyczka M., Tohline J. E., 1990, ApJ, 355, 651
Boss A. P., 1997, Science, 276, 1836
Boss A. P., 1998, ApJ, 503, 923
Bowler B. P. et al., 2010, ApJ, 709, 396
Brauer F., Dullemond C. P., Henning T., 2008, A&A, 480, 859
Cadman J., Hall C., Rice K., Harries T. J., Klaassen P. D., 2020a, MNRAS, 498, 4256
Cadman J., Rice K., Hall C., Haworth T. J., Biller B., 2020b, MNRAS, 492, 5041
Clarke C. J., 2009, MNRAS, 396, 1066
Cleary P. W., Monaghan J. J., 1999, J. Comput. Phys., 148, 227
Corder S., Eisner J., Sargent A., 2005, ApJ, 622, L133
DeWarf L. E., Sepinsky J. F., Guinan E. F., Ribas I., Nadalin I., 2003, ApJ, 590, 357
Dipierro G. et al., 2018, MNRAS, 475, 5296
Dipierro G., Pinilla P., Lodato G., Testi L., 2015, MNRAS, 451, 974
Dong R. et al., 2018, ApJ, 860, 124
Draine B. T., 2006, ApJ, 636, 1114
Durisen R. H., Boss A. P., Mayer L., Nelson A. F., Quinn T., Rice W. K. M., 2007, Protostars and Planets V. University of Arizona Press, Tucson, AZ
Dutrey A. et al., 2014, Protostars and Planets VI. Univ. Arizona Press, Tucson, AZ
Forgan D., Rice K., 2011, MNRAS, 417, 1928
Forgan D., Rice K., 2013a, MNRAS, 430, 2082
Forgan D., Rice K., 2013b, MNRAS, 432, 3168
Forgan D., Rice K., Stamatellos D., Whitworth A., 2009, MNRAS, 394, 882
Forgan D. H., Hall C., Meru F., Rice W. K. M., 2018, MNRAS, 474, 5036
Gaia Collaboration et al., 2018, A&A, 616, A1
Gammie C. F., 2001, ApJ, 553, 174
Garufi A. et al., 2013, A&A, 560, A105
Ginski C. et al., 2016, A&A, 595, A112
Grady C. A. et al., 2013, ApJ, 762, 48
Greenzweig Y., Lissauer J. J., 1992, Icarus, 100, 440
Haffert S. Y., Bohn A. J., de Boer J., Snellen I. A. G., Brinchmann J., Girard J. H., Keller C. U., Bacon R., 2019, Nat. Astron., 3, 749
Haisch Karl E. J., Lada E. A., Lada C. J., 2001, ApJ, 553, L153
Hall C. et al., 2020, ApJ, 904, 8
Hall C., Forgan D., Rice K., 2017, MNRAS, 470, 2517
Hall C., Dong R., Rice K., Harries T. J., Najita J., Alexander R., Brittain S., 2019, ApJ, 871, 228
Hartmann L., Calvet N., Gullbring E., D'Alessio P., 1998, ApJ, 495, 385
Hashimoto J. et al., 2011, ApJ, 729, L17
Haworth T. J., Cadman J., Meru F., Hall C., Albertini E., Forgan D., Rice K., Owen J. E., 2020, MNRAS, 494, 4130
Huang J. et al., 2018a, ApJ, 869, L42
Huang J. et al., 2018b, ApJ, 869, L43
Hubeny I., 1990, ApJ, 351, 632
Humphries J., Vazan A., Bonavita M., Helled R., Nayakshin S., 2019, MNRAS, 488, 4873
Ida S., Lin D. N. C., 2004, ApJ, 604, 388
Ikoma M., Nakazawa K., Emori H., 2000, ApJ, 537, 1013
Ilee J. D., Hall C., Walsh C., Jiménez-Serra I., Pinte C., Terry J., Bourke T., Hoare M., 2020, MNRAS, 498, 5116
Johansen A., Lambrechts M., 2017, Annu. Rev. Earth Planet. Sci., 45, 359
Johansen A., Oishi J. S., Mac Low M.-M., Klahr H., Henning T., Youdin A., 2007, Nature, 448, 1022
Johansen A., Klahr H., Henning T., 2011, A&A, 529, A62
Johansen A., Youdin A. N., Lithwick Y., 2012, A&A, 537, A125
Johnson J. A. et al., 2007, ApJ, 665, 785
Keppler M. et al., 2018, A&A, 617, A44
Kratter K. M., Murray-Clay R. A., Youdin A. N., 2010, ApJ, 710, 1375
Lynden-Bell D., Pringle J. E., 1974, MNRAS, 168, 603
Marois C., Macintosh B., Barman T., Zuckerman B., Song I., Patience J., Lafrenière D., Doyon R., 2008, Science, 322, 1348
Marois C., Zuckerman B., Konopacky Q. M., Macintosh B., Barman T., 2010, Nature, 468, 1080
Mayer L., Lufkin G., Quinn T., Wadsley J., 2007, ApJ, 661, L77
Mizuno H., 1980, Prog. Theor. Phys., 64, 544
Mordasini C., Klahr H., Alibert Y., Benz W., Dittkrist K.-M., 2010, Proceedings Circumstellar disks and planets, May 26-28, 2010, Kiel. Preprint (arXiv:1012.5281)
Müller A. et al., 2018, A&A, 617, L2
Nayakshin S., 2010a, MNRAS, 408, L36
Nayakshin S., 2010b, MNRAS, 408, 2381
Nayakshin S., 2011, MNRAS, 413, 1462
Nayakshin S., Fletcher M., 2015, MNRAS, 452, 1654
Nero D., Bjorkman J. E., 2009, ApJ, 702, L163
Nielsen E. L. et al., 2019, AJ, 158, 13
Owen J. E., Ercolano B., Clarke C. J., 2011, MNRAS, 412, 13
Perez S. et al., 2015, ApJ, 798, 85
Pérez L. M. et al., 2016, Science, 353, 1519
Piétu V., Guilloteau S., Dutrey A., 2005, A&A, 443, 945
Pollack J. B., Hubickyj O., Bodenheimer P., Lissauer J. J., Podolak M., Greenzweig Y., 1996, Icarus, 124, 62
Price D. J. et al., 2018, Publ. Astron. Soc. Aust., 35, e031
Pringle J. E., 1981, ARA&A, 19, 137
Rafikov R. R., 2005, ApJ, 621, L69
Rafikov R. R., 2017, ApJ, 837, 163
Rice W. K. M., Armitage P. J., 2009, MNRAS, 396, 2228
Rice W. K. M., Lodato G., Pringle J. E., Armitage P. J., Bonnell I. A., 2004, MNRAS, 355, 543

Rice W. K. M., Lodato G., Armitage P. J., 2005, MNRAS, 364, L56
Rice W. K. M., Lodato G., Pringle J. E., Armitage P. J., Bonnell I. A., 2006, MNRAS, 372, L9
Safronov V., 1969, Evolution of the Protoplanetary Cloud and Formation of the Earth and the Planets, English translation (1972)
Salyk C., Herczeg G. J., Brown J. M., Blake G. A., Pontoppidan K. M., van Dishoeck E. F., 2013, ApJ, 769, 21
Semenov D., Pavlyuchenkov Y., Schreyer K., Henning T., Dullemond C., Bacmann A., 2005, ApJ, 621, 853
Shakura N. I., Sunyaev R. A., 1973, A&A, 500, 33
Stamatellos D., Whitworth A. P., Bisbas T., Goodwin S., 2007, A&A, 475, 37
Tang Y. W., Guilloteau S., Piétu V., Dutrey A., Ohashi N., Ho P. T. P., 2012, A&A, 547, A84
Tang Y.-W. et al., 2017, ApJ, 840, 32
Testi L. et al., 2014, Protostars and Planets VI, Univ. Arizona Press, Tucson, AZ
Toomre A., 1964, ApJ, 139, 1217
van Boekel R. et al., 2017, ApJ, 837, 132
van den Ancker M. E., The P. S., Tjin A Djie H. R. E., Catala C., de Winter D., Blondel P. F. C., Waters L. B. F. M., 1997, A&A, 324, L33
Vigan A. et al., 2017, A&A, 603, A3
Weidenschilling S. J., 1977, MNRAS, 180, 57
Whitworth A. P., Stamatellos D., 2006, A&A, 458, 817
Williams J. P., Cieza L. A., 2011, ARA&A, 49, 67
Youdin A. N., Goodman J., 2005, ApJ, 620, 459
Youdin A., Johansen A., 2007, ApJ, 662, 613
Zsom A., Ormel C. W., Güttler C., Blum J., Dullemond C. P., 2010, A&A, 513, A57

This paper has been typeset from a TEX/LATEX file prepared by the author.

List of astronomical key words (Updated on 2020 January)

This list is common to *Monthly Notices of the Royal Astronomical Society, Astronomy and Astrophysics*, and *The Astrophysical Journal*. In order to ease the search, the key words are subdivided into broad categories. No more than *six* subcategories altogether should be listed for a paper.

The subcategories in boldface containing the word 'individual' are intended for use with specific astronomical objects; these should never be used alone, but always in combination with the most common names for the astronomical objects in question. Note that each object counts as one subcategory within the allowed limit of six.

The parts of the key words in italics are for reference only and should be omitted when the keywords are entered on the manuscript.

General
editorials, notices
errata, addenda
extraterrestrial intelligence
history and philosophy of astronomy
miscellaneous
obituaries, biographies
publications, bibliography
sociology of astronomy
standards

Physical data and processes
acceleration of particles
accretion, accretion discs
asteroseismology
astrobiology
astrochemistry
astroparticle physics
atomic data
atomic processes
black hole physics
chaos
conduction
convection
dense matter
diffusion
dynamo
elementary particles
equation of state
gravitation
gravitational lensing: micro
gravitational lensing: strong
gravitational lensing: weak
gravitational waves
hydrodynamics
instabilities
line: formation
line: identification
line: profiles
magnetic fields
magnetic reconnection
(magnetohydrodynamics) MHD
masers
molecular data
molecular processes
neutrinos
nuclear reactions, nucleosynthesis, abundances
opacity
plasmas
polarization
radiation: dynamics
radiation mechanisms:general
radiation mechanisms: non-thermal
radiation mechanisms: thermal
radiative transfer
relativistic processes
scattering
shock waves
solid state: refractory
solid state: volatile
turbulence
waves

Astronomical instrumentation, methods and techniques
atmospheric effects
balloons
instrumentation: adaptive optics
instrumentation: detectors
instrumentation: high angular resolution
instrumentation: interferometers
instrumentation: miscellaneous
instrumentation: photometers
instrumentation: polarimeters
instrumentation: spectrographs
light pollution
methods: analytical
methods: data analysis
methods: laboratory: atomic
methods: laboratory: molecular
methods: laboratory: solid state
methods: miscellaneous
methods: numerical
methods: observational
methods: statistical
site testing
space vehicles
space vehicles: instruments
techniques: high angular resolution
techniques: image processing
techniques: imaging spectroscopy
techniques: interferometric
techniques: miscellaneous
techniques: photometric
techniques: polarimetric
techniques: radar astronomy
techniques: radial velocities
techniques: spectroscopic
telescopes

Astronomical data bases
astronomical data bases: miscellaneous
atlases
catalogues
surveys
virtual observatory tools

Software
software: data analysis
software: development
software: documentation
software: public release
software: simulations

Astrometry and celestial mechanics
astrometry
celestial mechanics
eclipses
ephemerides
occultations
parallaxes
proper motions
reference systems
time

The Sun
Sun: abundances
Sun: activity
Sun: atmosphere
Sun: chromosphere
Sun: corona
Sun: coronal mass ejections (CMEs)
Sun: evolution
Sun: faculae, plages
Sun: filaments, prominences
Sun: flares
Sun: fundamental parameters
Sun: general
Sun: granulation
Sun: helioseismology
Sun: heliosphere
Sun: infrared
Sun: interior
Sun: magnetic fields
Sun: oscillations
Sun: particle emission
Sun: photosphere
Sun: radio radiation
Sun: rotation
(Sun:) solar–terrestrial relations
(Sun:) solar wind
(Sun:) sunspots
Sun: transition region
Sun: UV radiation
Sun: X-rays, gamma-rays

Planetary systems
comets: general

comets: individual: . . .
Earth
interplanetary medium
Kuiper belt: general

Kuiper belt objects: individual: . . .
meteorites, meteors, meteoroids
minor planets, asteroids: general

minor planets, asteroids: individual: . . .
Moon
Oort Cloud
planets and satellites: atmospheres
planets and satellites: aurorae
planets and satellites: composition
planets and satellites: detection
planets and satellites: dynamical evolution and stability
planets and satellites: formation
planets and satellites: fundamental parameters
planets and satellites: gaseous planets
planets and satellites: general

planets and satellites: individual: . . .
planets and satellites: interiors
planets and satellites: magnetic fields
planets and satellites: oceans
planets and satellites: physical evolution
planets and satellites: rings
planets and satellites: surfaces
planets and satellites: tectonics
planets and satellites: terrestrial planets
planet–disc interactions
planet–star interactions
protoplanetary discs
zodiacal dust

Stars
stars: abundances
stars: activity
stars: AGB and post-AGB
stars: atmospheres
(stars:) binaries *(including multiple)*: close
(stars:) binaries: eclipsing
(stars:) binaries: general
(stars:) binaries: spectroscopic
(stars:) binaries: symbiotic
(stars:) binaries: visual
stars: black holes
(stars:) blue stragglers
(stars:) brown dwarfs
stars: carbon
stars: chemically peculiar
stars: chromospheres
(stars:) circumstellar matter
stars: coronae
stars: distances
stars: dwarf novae
stars: early-type
stars: emission-line, Be
stars: evolution
stars: flare
stars: formation
stars: fundamental parameters
(stars:) gamma-ray burst: general
(stars:) **gamma-ray burst: individual: . . .**
stars: general
(stars:) Hertzsprung–Russell and colour–magnitude diagrams
stars: horizontal branch
stars: imaging
stars: individual: . . .
stars: interiors

stars: jets
stars: kinematics and dynamics
stars: late-type
stars: low-mass
stars: luminosity function, mass function
stars: magnetars
stars: magnetic field
stars: massive
stars: mass-loss
stars: neutron
(stars:) novae, cataclysmic variables
stars: oscillations *(including pulsations)*
stars: peculiar *(except chemically peculiar)*
(stars:) planetary systems
stars: Population II
stars: Population III
stars: pre-main-sequence
stars: protostars
(stars:) pulsars: general
(stars:) **pulsars: individual: . . .**
stars: rotation
stars: solar-type
(stars:) starspots
stars: statistics
(stars:) subdwarfs
(stars:) supergiants
(stars:) supernovae: general
(stars:) **supernovae: individual: . . .**
stars: variables: Cepheids
stars: variables: Scuti
stars: variables: general
stars: variables: RR Lyrae
stars: variables: S Doradus
stars: variables: T Tauri, Herbig Ae/Be
(stars:) white dwarfs
stars: winds, outflows
stars: Wolf–Rayet

Interstellar medium (ISM), nebulae
ISM: abundances
ISM: atoms
ISM: bubbles
ISM: clouds
(ISM:) cosmic rays
(ISM:) dust, extinction
ISM: evolution
ISM: general
(ISM:) HII regions
(ISM:) Herbig–Haro objects

ISM: individual objects: . . .
(except planetary nebulae)
ISM: jets and outflows
ISM: kinematics and dynamics
ISM: lines and bands
ISM: magnetic fields
ISM: molecules
(ISM:) photodissociation region (PDR)
(ISM:) planetary nebulae: general
(ISM:) **planetary nebulae: individual: . . .**
ISM: structure
ISM: supernova remnants

The Galaxy
Galaxy: abundances
Galaxy: bulge
Galaxy: centre
Galaxy: disc
Galaxy: evolution
Galaxy: formation
Galaxy: fundamental parameters
Galaxy: general
(Galaxy:) globular clusters: general
(Galaxy:) **globular clusters: individual: . . .**
Galaxy: halo
Galaxy: kinematics and dynamics
(Galaxy:) local interstellar matter
Galaxy: nucleus
(Galaxy:) open clusters and associations: general
(Galaxy:) **open clusters and associations: individual: . . .**
(Galaxy:) solar neighbourhood
Galaxy: stellar content
Galaxy: structure

Galaxies
galaxies: abundances
galaxies: active
galaxies: bar
(galaxies:) BL Lacertae objects: general
(galaxies:) **BL Lacertae objects: individual: . . .**
galaxies: bulges
galaxies: clusters: general

galaxies: clusters: individual: . . .
galaxies: clusters: intracluster medium
galaxies: disc
galaxies: distances and redshifts
galaxies: dwarf
galaxies: elliptical and lenticular, cD
galaxies: evolution
galaxies: formation
galaxies: fundamental parameters
galaxies: general
galaxies: groups: general

galaxies: groups: individual: . . .
galaxies: haloes
galaxies: high-redshift

galaxies: individual: . . .
galaxies: interactions
(galaxies:) intergalactic medium
galaxies: irregular
galaxies: ISM
galaxies: jets
galaxies: kinematics and dynamics
(galaxies:) Local Group
galaxies: luminosity function, mass function
(galaxies:) Magellanic Clouds
galaxies: magnetic fields
galaxies: nuclei
galaxies: peculiar
galaxies: photometry
(galaxies:) quasars: absorption lines
(galaxies:) quasars: emission lines
(galaxies:) quasars: general

(galaxies:) **quasars: individual: . . .**
(galaxies:) quasars: supermassive black holes
galaxies: Seyfert
galaxies: spiral
galaxies: starburst
galaxies: star clusters: general

galaxies: star clusters: individual: . . .
galaxies: star formation
galaxies: statistics
galaxies: stellar content
galaxies: structure

Cosmology
(cosmology:) cosmic background radiation
(cosmology:) cosmological parameters
(cosmology:) dark ages, reionization, first stars
(cosmology:) dark energy
(cosmology:) dark matter
(cosmology:) diffuse radiation
(cosmology:) distance scale
(cosmology:) early Universe
(cosmology:) inflation
(cosmology:) large-scale structure of Universe
cosmology: miscellaneous
cosmology: observations
(cosmology:) primordial nucleosynthesis
cosmology: theory

Resolved and unresolved sources as a function of wavelength
gamma-rays: diffuse background
gamma-rays: galaxies
gamma-rays: galaxies: clusters
gamma-rays: general
gamma-rays: ISM
gamma-rays: stars
infrared: diffuse background
infrared: galaxies
infrared: general
infrared: ISM
infrared: planetary systems
infrared: stars
radio continuum: galaxies
radio continuum: general
radio continuum: ISM
radio continuum: planetary systems
radio continuum: stars
radio continuum: transients
radio lines: galaxies
radio lines: general
radio lines: ISM
radio lines: planetary systems
radio lines: stars
submillimetre: diffuse background
submillimetre: galaxies
submillimetre: general
submillimetre: ISM
submillimetre: planetary systems
submillimetre: stars
ultraviolet: galaxies
ultraviolet: general
ultraviolet: ISM
ultraviolet: planetary systems
ultraviolet: stars
X-rays: binaries
X-rays: bursts
X-rays: diffuse background
X-rays: galaxies
X-rays: galaxies: clusters
X-rays: general
X-rays: individual: . . .
X-rays: ISM
X-rays: stars

Transients
(transients:) black hole mergers
(transients:) black hole - neutron star mergers
(transients:) fast radio bursts
(transients:) gamma-ray bursts
(transients:) neutron star mergers
transients: novae
transients: supernovae
transients: tidal disruption events